Kinetic Insights into Li x Ni 0.67 N ($1.67 \leq x \leq 2.17$), a quasi "Zero-Strain" Negative Electrode Material for Li-Ion Battery

Yanlong Zhou, Nicolas Emery, Sylvain Franger, Olivier Nguyen, Jean Pierre Pereira-Ramos, Rita Baddour-Hadjean

Kinetic Insights into $Li_xNi_{0.67}N$ ($1.67 \leq x \leq 2.17$), a quasi "Zero-Strain" Negative Electrode Material for Li-Ion Battery

Y.Zhou[1,2*], N. Emery[1], S. Franger[3], O. Nguyen[2], J.P. Pereira-Ramos[1*], R. Baddour-Hadjean[1]

[1] Institut de Chimie et des Matériaux Paris Est (ICMPE-CNRS), UMR 7182 CNRS-Université Paris-Est Créteil, 2 rue Henri-Dunant 94320 Thiais, France

[2] Technocentre Renault, 1 Avenue du Golf, 78280 Guyancourt, France

[3] Institut de Chimie Moléculaire et des Matériaux d'Orsay (ICMMO-CNRS), UMR 8182 CNRS-Université Paris-Saclay, 410 Rue du Doyen Georges Poitou, 91405 Orsay, France

Abstract

The kinetics of the electrochemical lithium intercalation in the nitridonickelate $Li_xNi_{0.67}N$ ($1.67 \leq x \leq 2.17$) is investigated by electrochemical impedance spectroscopy during a full reduction-oxidation cycle in a two-electrode cell. The layered structure of this anode material delivers a reversible and stable specific capacity of 200 mAh g^{-1} over 100 cycles at C/10 near 0.5 V vs Li^+/Li. The equivalent electric circuit simulation allows a full assignment of the impedance spectra, with different contributions including the SEI layers on each electrode, charge transfer and Li diffusion. The calculated lithium diffusion coefficient value of approximately 5×10^{-9} cm ^{2} s^{-1} almost does not vary with the lithium content in $Li_xNi_{0.67}N$ ($1.67 \leq x \leq 2.17$). Conversely, the charge transfer resistance (R_{ct}) is found to strongly depend on the depth of reduction to be maximum for the fully reduced electrode, with a totally reversible behavior during oxidation. The overall impedance of the cell remains stable upon long cycling, which indicates a good chemical stability of the SEI on $Li_xNi_{0.67}N$ as well as

remarkable structural and chemical stability of the nitridonickelate upon cycles. The present kinetic findings shed light on the remarkable "zero-strain" behavior of this negative electrode material presenting numerous Li vacancies.

Keywords: Lithiated nickel nitride, Li-ion batteries, anode, kinetics study, impedance spectroscopy, Lithium diffusion coefficient

1. Introduction

Li-ion battery (LiBs) is one of most important energy storage technologies to help human society for the energy transition. Since the introduction of LiBs, great efforts have been made to explore new anode materials to circumvent the disadvantages of graphite [1–5]. With lower working potential than oxides, lithium transition-metal nitrides have been proposed as promising anode materials for Li-ion battery since 1997 [6–14]. Two types of structure can be found in the family of lithium transition-metal nitrides: anti-fluorite 3D structures such as Li_7MnN_4 [6–8], and Li_3N-type layered structure with a general formula $Li_{3-xy}M_xN$ (M = Co, Ni, Cu; y = oxidation state of metal) [9–14]. Among these layered ternary transition metal nitrides, $Li_{2.6}Co_{0.4}N$ received special attention due to its large capacity of 480-800 mAh/g available in the 1.4 V-0 V vs Li^+/Li potential range. However, $Li_{2.6}Co_{0.4}N$ exhibits significant capacity fading upon cycling due to a conversion mechanism [15] involving an irreversible structural change toward an amorphous phase during the first Li extraction process. Numerous efforts have been made to improve the cycling performance of $Li_{2.6}Co_{0.4}N$ by using composite anodes with suitable electrode binder and electronic conductor (hard carbon, nano-oxides or nanosized alloys) [16–19].

Recently, our group has demonstrated the existence of genuine Li intercalation compounds in the Li-Co-N system ($Li_{3-2x}Co_xN$, $0.1 \leq x \leq 0.44$) [14] and in the Li-Ni-N system ($Li_{3-2x}Ni_xN$, $0.2 \leq x \leq 0.6$) [13,20]. Nitridonickelate-based compounds, with general formula $Li_{3-xy}Ni_xN$ ($1 \leq y \leq 2$, referred as Ni oxidation state; $0.20 \leq x \leq 0.67$, referred as Ni content), exhibits a capacity of 120-200 mAh g^{-1} in the 1.25 V-0.02 V potential range combined with good cycling performance. In the Li-Ni-N system, $Li_{2.0}Ni_{0.67}N$ (LNN) with the highest Ni content was identified as the most promising composition, providing the highest specific capacity of 200 $mAhg^{-1}$ available at an average working potential of 0.5 V [21]. Moreover, as demonstrated in this work, LNN exhibits almost 100% capacity retention upon cycling at C/10 and more than 88% at 1C over at least 100 cycles. Such remarkable cycling properties were ascribed to the "zero-strain" structural behavior of LNN upon cycling [21], the structural response of LNN during reduction and oxidation consisting in a solid solution behavior involving the Ni^{2+}/Ni^{+} redox couple, with reversible accommodation of Li^{+} ions in the numerous cationic vacancies of its stable hexagonal structure. Such original structural behavior of LNN associated to the promising electrochemical properties of this anode material deserves a detailed kinetics investigation, which to our knowledge, has not yet been conducted for the nitridonickelate system.

Here we report a comprehensive kinetic study of the LNN material, using electrochemical impedance spectroscopy (EIS). The kinetic parameters of the electrochemical Li insertion-extraction reaction are investigated as a function of x in $Li_xNi_{0.67}N$ ($1.67 \leq x \leq 2.17$) as well as during cycling. The achieved findings allow getting a full understanding of the remarkable electrochemical properties of this promising anode for LIBs.

2. Experimental

$Li_{2.0}Ni_{0.67}N$ was synthesized by a solid-state reaction under nitrogen flow. Since lithiated transition metal nitrides are sensitive to moisture[22,23], all the operations were carried out in an Ar-filled glove box ($p(H_2O)$, $p(O_2)$ < 0.1ppm). Around 1 g of metallic Ni and Li_3N (Alfa-Aesar, −60 mesh, 99.4%) powders were thoroughly mixed in an agate mortar with a molar ratio 1:1. The mixture was pressed into a pellet with a diameter of 13 mm under a pressure of 10^3 kg cm^{-2}. The pellet was then transferred into an alumina crucible placed inside an airtight tubular stainless-steel reactor. Two other crucibles containing titanium sponges were placed next to the crucible containing the pellet to trap oxygen traces and moisture during the reaction. The stainless-steel reactor was then heated to 720 °C in a tubular oven under a continuous nitrogen flow of 0.1 L min^{-1}. After the heat treatment, the sintered pellet was hand ground into fine power during 15 min in an agate mortar inside the glove box.

The XRD pattern of the as prepared powder was collected using a Panalytical X'pert pro diffractometer equipped with a Co K_α source and X'celerator detector. A semi-sphere polymer airtight sample holder was used to keep the material inside an inert atmosphere. The Rietveld refinement was performed using GSAS package with the EXPGUI interface [24,25]. The atomic displacement parameters U_{iso} were constrained to be the same for the cations.

Electrochemical impedance measurements were carried out in a two-electrode CR2032 coin cell, using a Biologic VMP3 apparatus. The ground $Li_{2.0}Ni_{0.67}N$ powder was mixed with acetylene black (22% wt) and PTFE (8% wt) and then rolled into a thin sheet. A round shape sheet (8 mm in diameter) was cut out and pressed under 10^3 kg cm^{-2} onto a copper grid (12 mm in diameter) acting as working electrode (geometric area of 0.5 cm^2). A metallic lithium

disk (16 mm in diameter) was used as counter and reference electrode. The electrolyte was 1 mol L^{-1} $LiPF_6$ in ethylene carbonate (EC), diethyl carbonate (DEC) and dimethyl carbonate (DMC) solution (1:1:1, Alfar-Aesar). Glass microfiber filter paper (Whatman™, grade GF/A) was used as separator. The impedance study was carried out in the 10^6 Hz - $2 \cdot 10^{-3}$ Hz frequency range. The excitation signal was 7 mV peak to peak. The equilibrium potential was considered to be reached when the potential change in open circuit voltage remained less than 1 mV/h. Operando XRD experiments were carried out in a special designed electrochemical cell with a beryllium window. Full reduction/oxidation cycles in the special electrochemical cell were performed at C/20 rate (i.e., 1 Li^+ exchanged in 20 h) using a Biologic VSP150 apparatus. The Be window acts as both current collector and X-ray transparent window. The separator, electrolyte, counter and working electrodes were identical to those described above for the coin cell. The thin sheet of working electrode was pressed onto a copper grid and directly placed under the Be window. In terms of results analyses, the environment contributions such as the Be window or the copper grid were fitted with the Le Bail method.

Chemical composition was determined by ion beam analysis (IBA), including Rutherford backscattering (RBS) and nuclear reaction analysis (NRA). An IBA experiment was performed with a 3.03 MeV H^+ beam produced by the Van de Graaf accelerator of the IRAMIS/LEEL at CEA-Saclay, and the spectrum was collected using an annular detector, which covers backscattering angles centered around 170°.

3. Results and discussion

3.1. Structural characterization

The Rietveld refinement of the as synthesized LNN XRD pattern is displayed in **Figure 1a**. All the peaks are indexed in a hexagonal symmetry, space group *P6/mmm*, with the following unit cell parameters a = 3.760(1) Å and c = 3.540(2) Å and refinement statistics parameters χ^2= 8.12; R_p = 2.9%; R_{wp} = 5.5%. These data reveal our synthesis leads to a pure nitridonickelate phase with a chemical composition $Li_{2.0}Ni_{0.67}N$ (LNN), in good agreement with our previous work [21]. The schematic layered structure of LNN is shown in **Figure 1b**. Nitrogen anions sit in the *1a* sites while Ni and Li cations occupy the *1b* interlayer sites. While the *2c* site is fully occupied by lithium ions in Li_3N, the Li site occupation in the Li-Ni-N system depends on the oxidation state of Ni. The chemical composition of the present nitridonickelate was determined as $Li_{2.0}Ni_{0.67}N$ from RBS experiments [21]. This implies an intermediate Ni valence near +1.5 (i.e. 0.33 Ni^{2+} and 0.33 Ni^{+} per mole of nitride) as well as the existence of 0.33 Li vacancies in the *2c* sites located in the nitrogen planes.

The SEM images of the pristine LNN powder show that this compound is made of hexagonal platelets with an average size of 10 µm (**Figure 1c**).

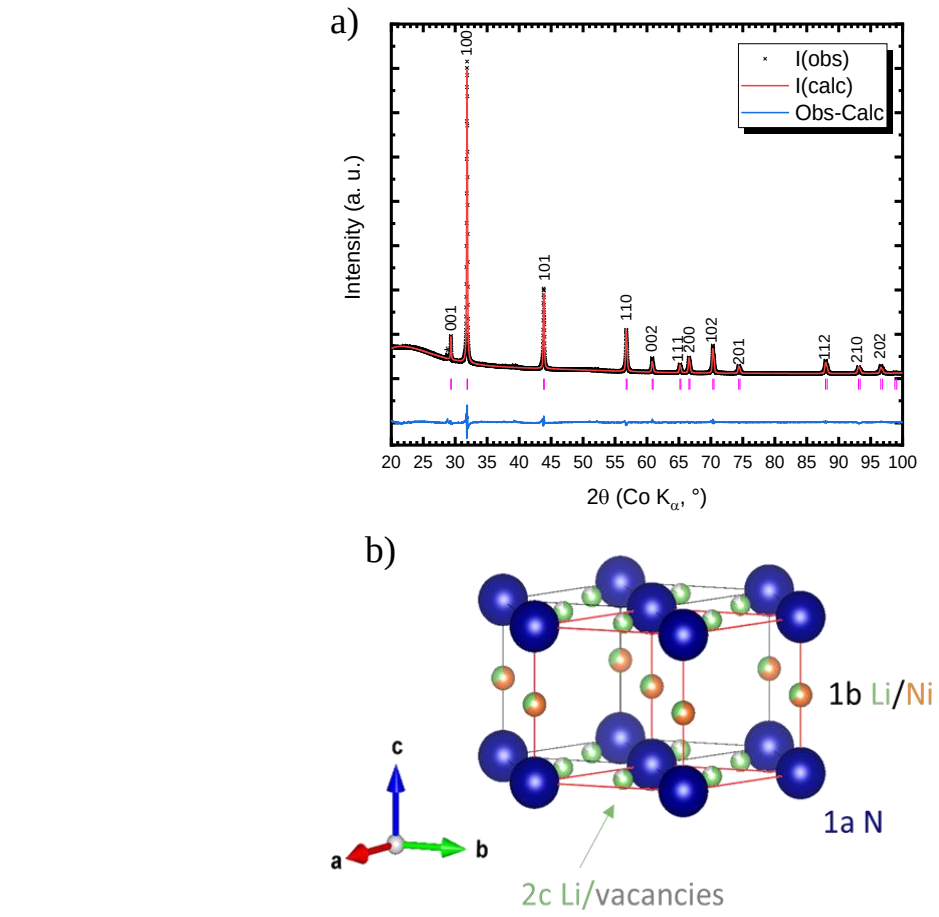

Figure 1. a) Rietveld refinement of the XRD pattern (χ^2= 8.12; R_p=2.9%; R_{wp}=5.5%) and b) representation of the crystalline structure of the pristine LNN powder. Nitrogen anions (blue spheres) nickel ions (orange spheres) lithium ions (green spheres). c) SEM images of the pristine LNN powder.

3.2. Electrochemical characterization

The attractive electrochemical properties of LNN are illustrated in **Figure 2**. At C/10, the sloping shape of the typical reduction-oxidation curve indicates a single step electrochemical process involving the exchange of 0.5 lithium ions (**Figure 2a**). As expected from this peculiar profile, a solid solution behavior was previously revealed from operando XRD measurements [21], with very limited structure breathing, the *a* and *c* parameters varying in opposite direction by less than 2% for a maximum faradaic yield (FY) of 0.5 F per mole of nitride. The reduction-oxidation curve in **Figure 2a** also outlines the high reversibility of the reaction, characterized by a hysteresis value that never exceeds 100 mV. The PTFE binder used as mechanical agent was shown to be responsible for a reversible partial chemical oxidation [26–28] of $Li_{2.0}Ni_{0.67}N$ leading to $Li_{1.67}Ni_{0.67}N$, with lattice parameters a = 3.729 and c = 3.556 Å [21]. Hence, before starting the reduction, LNN contains only divalent Ni^{2+} ions and 0.67 Li vacancies while the fully reduced product corresponds to the chemical composition $Li_{2.17}Ni_{0.67}N$ (a = 3.771 Å; c = 3.745 Å) with about 0.17 Ni^{2+} and 0.5 Ni^{+}. A facile and reversible Li accommodation in the numerous Li vacancies located in *2c* sites takes place without any significant structural strain. The unit cell parameters for the different $Li_xNi_{0.67}N$ ($1.67 \leq x \leq 2.17$) compositions are calculated from the operando XRD study (**Figure S1**) and gathered in **Table 1.**

Composition	Unit cell parameter (*P6/mmm*)	
	a (Å)	*c* (Å)
$Li_{1.67}Ni_{0.67}N$, FY = 0	3.729 (*a*' = 6.459 Å) *	3.556
$Li_{2.0}Ni_{0.67}N$, FY = 0.33	3.760	3.540
$Li_{2.17}Ni_{0.67}N$, FY = 0.5	3.771	3.745

Table 1. Unit cell parameters in the *P6/mmm* space group of the pristine oxidized $Li_{1.67}Ni_{0.67}N$ electrode (FY = 0), as prepared $Li_{2.0}Ni_{0.67}N$ powder (FY = 0.33) and fully reduced electrode (FY = 0.5). * The pristine $Li_{1.67}Ni_{0.67}N$ electrode is indexed within the *P-62m* space group, which leads to a 3-time larger supercell [21], for an easier comparison, the unit cell parameter was recalculated in *P6/mmm* space group (a = a' / $3^{1/2}$).

A meaningful illustration of the advantageous zero-strain properties of the present nitridonickelate electrode is provided by its excellent cycle life behavior, with a remarkable capacity stability of 200 mAh g^{-1} over at least 100 cycles at C/10 in the 1.25 V-0.02 V range (**Figure 2b)**. A good capacity retention is also observed at higher C-rate, with however a slight capacity decline from 130 to 115 mAh g^{-1} after 100 cycles at 1C (**Figure 2b**). The rate capability study (**Figure 2c-2d)** also points to an excellent capacity retention of the LNN nitride whatever the applied C-rate in the C/20–2C (20–800 mA/g). High capacity values are reached: 200 mAh g^{-1} at C/10, 180 mAh g^{-1} at C/5, 150 mAh g^{-1} at C/2, still 110 mAh g^{-1} at C and 70 mAh g^{-1} at 2C. Even after applying 2C for 20 cycles, the initial capacity of 200 mAh g^{-1} can be recovered, showing the absence of any detrimental effect by applying high current densities.

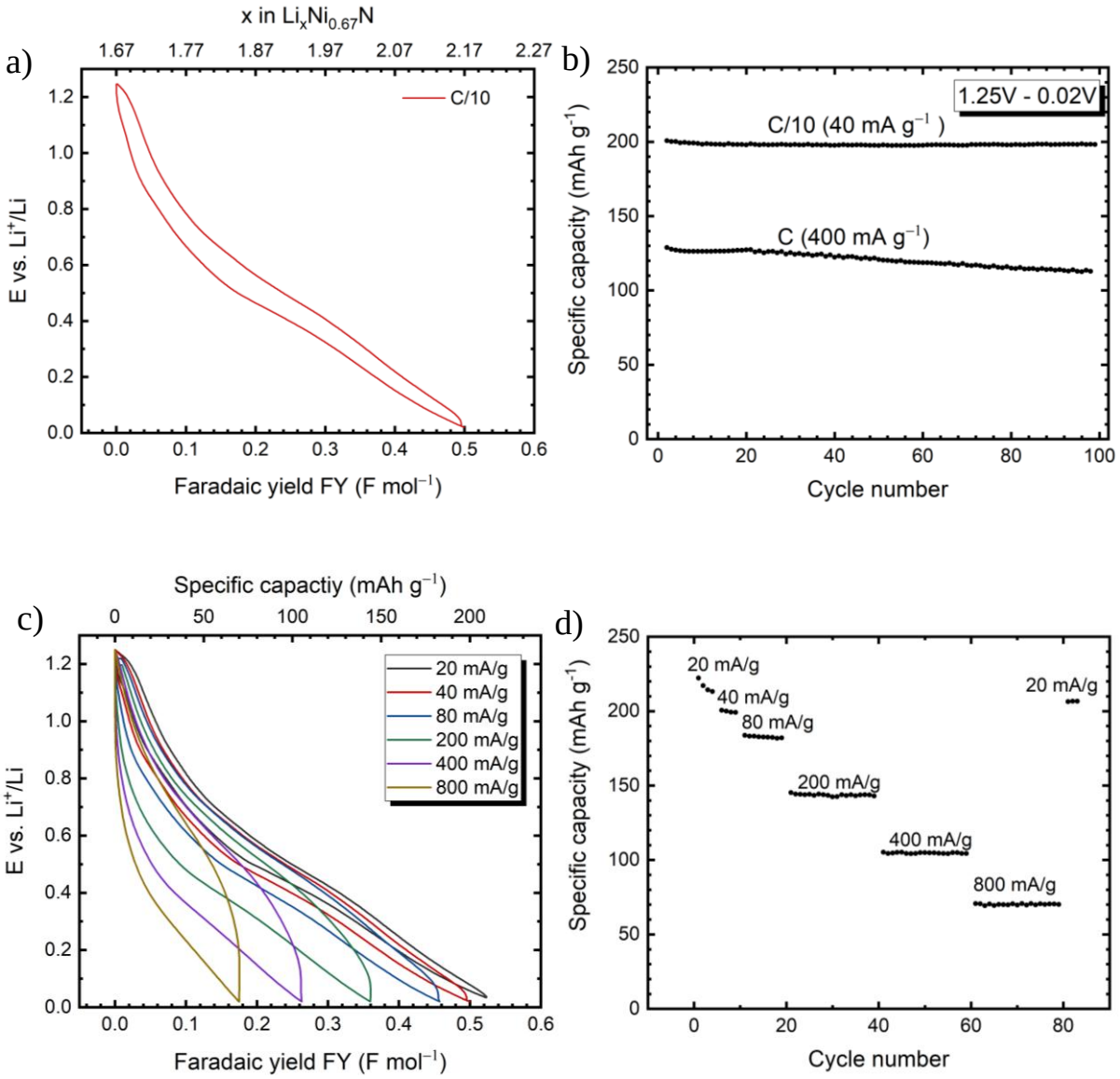

Figure 2. Electrochemical properties of LNN in the 1.25 V–0.02 V voltage range; (a) Typical reduction-oxidation profile at C/10; (b) Evolution of the specific capacity vs number of cycles at C/10 (40 mA g^{-1}) and 1C (400 mA g^{-1}) rates; (c) and (d) Rate capability study.

It is worth comparing the present electrochemical performance with those reported for the challenging spinel lithium titanate $Li_4Ti_5O_{12}$ (LTO) anode material [8, 27–29]. First, the maximum capacity delivered by the lithiated nitridonickelate exceeds that of LTO that is limited to 175 mAh g^{-1}. Taking into account the significantly different molar weights (64.91 g mol^{-1} for LNN and 459.09 g mol^{-1} for LTO) and different Li uptakes (0.5 for LNN and 3 for LTO), a straightforward comparison relying on current density values leads to a systematically larger capacity of LNN than LTO when the current density doesn't exceed 200 mA g^{-1}, **Figure S2** [30]. More importantly, the lower operating voltage of LNN (0.5 V against 1.5 V for LTO) allows higher gravimetric energy density to be reached. Further studies on the optimization of the composite LNN electrode formulation/preparation by carbon coating or by using appropriate conductive additive such as graphene or CNT should allow to enhance the electronic conductivity of LNN and to compete with LTO even at high current densities.

3.3. Kinetics study

Despite unique structural features among the various Li intercalation compounds due to the presence of abundant cationic vacancies, the kinetics of Li transport in $Li_xNi_{0.67}N$ has never been addressed to our knowledge. The present study intends to give insights into the Li insertion-extraction mechanism by depicting the main kinetic reaction parameters as a function of the depth of reduction.

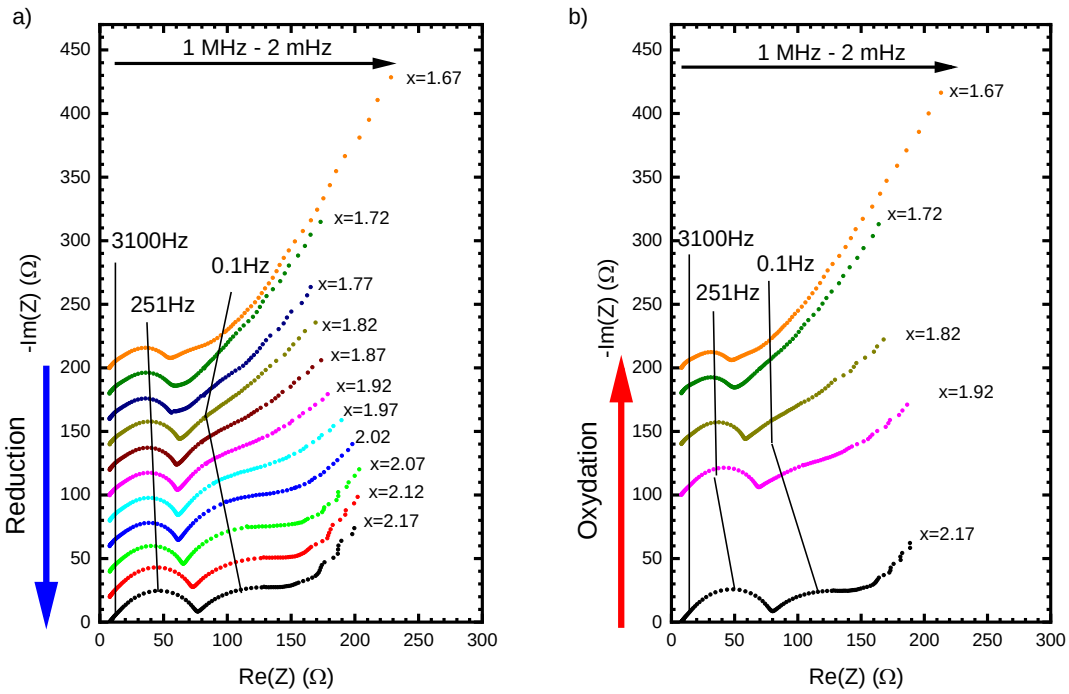

Figure 3. Evolution of the Nyquist diagrams of a LNN-Li cell as a function of x in $Li_xNi_{0.67}N$ during a) reduction (Li insertion) and b) oxidation (Li extraction).

The typical Nyquist diagrams of a LNN-Li cell as a function of the depth of reduction and oxidation in the range $1.67 \leq x \leq 2.17$ are gathered in **Figure 3**. A semicircle in the high frequency region (251 Hz) followed by a Warburg region in the medium frequency range and a capacitive line in the lower frequency region are representative of the starting material (x = 1.67) and the early stage of reduction (x = 1.72) (**Figure 3a**). For higher x values, while the semicircle located at 251 Hz remains unchanged, a new semicircle with a characteristic frequency of 0.1 Hz appears and grows continuously with x. Finally, this new contribution is very well defined for the fully reduced cell (x = 2.17). It is worth noting that the reverse trend

takes place upon oxidation, as revealed in **Figure 3b**. Indeed, the new semicircle is decreasing with decreasing x values and completely disappears for x = 1.67.

This reversible behavior evidenced from EIS experiments is in good agreement with the high structural [21] and electrochemical reversibility shown previously (**Figure 3a**). In addition, the lack of significant impedance variation between the fully oxidized and fully reduced states ($|Z|_{x=1.67}$ = 322 Ω, i.e., 161 Ω cm^2 $|Z|_{x=2.17}$ = 212 Ω, i.e., 106 Ω cm^2) confirms the promising properties of LNN as stable Li intercalation host lattice.

For a comprehensive understanding of the impedance spectra, a modeling has been performed for each x value upon reduction and oxidation. **Figure S3** shows three examples that illustrate how the modeling is performed during reduction (x = 1.67, x = 1.92 and x = 2.17). An expanded view of the first semicircle (f* = 251 Hz) indicates a shoulder at much higher frequency (3100 Hz) due to another relaxation phenomenon. A resistance/constant phase element (R_1/CPE_1) combination in parallel is used to account for the corresponding semicircle at 3100 Hz while another R_2/CPE_2 couple refers to the semicircle at 251 Hz. Finally, for frequencies lower than 10 Hz, a modified Randles equivalent circuit is used, including R_3/CPE_3 with a characteristic frequency of 0.1 Hz and a Warburg element. The CPE_4 with n = 0.5 is used to account for the Warburg element. The corresponding electric equivalent circuit used therefore consists of these three RC contributions in addition to R_0 (≈ 5 Ω cm^2) corresponding to the electrolyte resistance (**Figure S3**). The good agreement between experimental data (black points) and the modeling (blue curve) indicates the equivalent electric circuit used to depict the impedance diagrams is relevant. The simulation allowed us to extract values of R and C from the equivalent circuit. The evolutions of R_1, R_2 and R_3 vs x

are reported for the reduction process in **Figure 4**. The corresponding evolutions of C_1, C_2, C_3 are reported in **Figure S4**. While R_1 and R_2 remain practically unchanged along the insertion process with respectively a value of ≈ 5 Ω cm² and ≈ 14 Ω cm², R_3 is significantly changing with x, i.e with the Li and Ni^+ ions concentrations. More precisely, R_3 is continuously growing from x > 1.77, and then sharply increases from 2 Ω cm² for x = 1.82 to about 50 Ω cm² for x= 2.17. This finding strongly supports the fact that R_3 may be assigned to the charge transfer resistance of the reaction. The observed R_3 evolution indicates that the charge transfer kinetics ($R_{ct} = R_3$) is slowed down when the predominant nickel species are Ni^+ and promoted when Ni^{2+} ions dominate.

Let us consider now the other two semicircles with practically unchanged R_1 and R_2. The first dipole characterized by R_1 and C_1 corresponds to the SEI layer formed on Li metal, in good accord with our previous experiments made in a symmetric Li-Li coin cell with the same characteristic frequency of 3×10^3 Hz. The second contribution and main semicircle always observed and unchanged in frequency (at 251 Hz) and magnitude can be safely assigned to the SEI layer formed on the nitridonickelate.

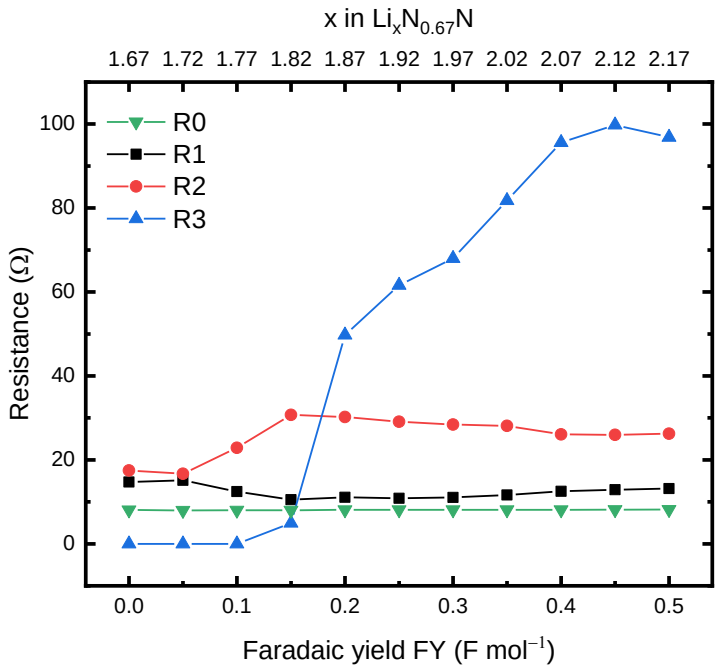

Figure 4. Evolution of R_1, R_2 and R_3 vs x in $Li_xNi_{0.67}N$ during the reduction process. Geometric Surface area of electrode is 0.5 cm^2

As seen from the first three galvanostatic cycles at C/10 (**Figure S5**), the coulombic efficiency is close to 50% for the first cycle, against 98% for the third one. This demonstrates the formation of a SEI layer on the nitride electrode, as expected for an anode material mainly working around 0.5 V vs Li^+/Li. The thickness of the SEI ($\boldsymbol{d = \varepsilon\varepsilon_0 S/C}$), which consists of a thin layer of ionic conductor, can be calculated from the capacitance values C_1 and C_2 and the relative permittivity known for the lithium SEI (mostly organic, ε_{Li} = 5) [32] and that of nitride SEI (mostly inorganic, ε_{LiF} = 9). Hence, d_1 and d_2 are found to be respectively equal to 2.3 nm and 1.6 nm and remain nearly unchanged along the reduction process. The corresponding resistivity $\boldsymbol{\rho = RS/d}$ can also be estimated in both cases**.** Highly resistive SEI

exists on lithium and LNN electrodes, but the latter is almost one order of magnitude more resistive (8.4×10^{-8} Ω cm) than the film formed on metallic lithium (1×10^{-8} Ω cm).

The Warburg region, where the value of imaginary impedance equals to the real impedance (-Im(Z) = Re (Z)) on the Nyquist diagram, can be easily identified by drawing a 45° line on the Re (Z) axis (**Figure S6**). This 45° portion of the line corresponds to a frequency range where the kinetics of the system is almost entirely limited by the rate of the diffusional process under semi-infinite conditions. In this domain, D_{Li} numerical values can be extracted using the following equation (Eq. (1)) when $\omega = 2\Pi f >> 2D_{Li}/L^2$: [33]

Equation 1:

$$D_{Li}^{+} = \left(\frac{V_m}{\sqrt{2}nFS} \cdot \frac{\Delta E}{\Delta x} \cdot \frac{1}{A_\omega}\right)^2$$

Where V_m is the molar volume (26.09 cm^3 mol^{-1}), dE/dx is the slope at fixed x of the equilibrium potential-composition curve (**Figure 5**), S is the apparent geometric area of the electrode (0.5 cm^2), A_ω is the Warburg prefactor (Ω $s^{-1/2}$), L is the maximum length of the diffusion pathway (cm).

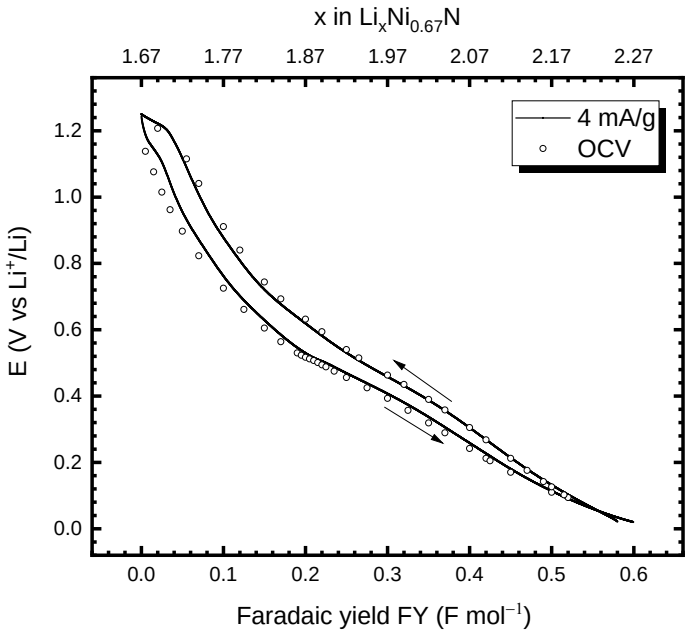

Figure 5. Open circuit voltage (OCV) data as a function of x in $Li_xNi_{0.67}N$ and galvanostatic reduction-oxidation curve at very low current density (C/100).

The analysis of the Warburg impedance plotted in the complex plane $Z' = A\ \omega^{-1/2}$ allows to get the Warburg prefactor A_ω (**Figure S7)** and then to calculate the apparent chemical lithium diffusion D_{Li} vs x, using equation 1. **Figure S7** shows that most of plotted straight lines for reduction exhibit relatively close slopes except for x = 1.67. This indicates in a first approach a low x dependence of Li diffusivity in the nitridonickelate. The evolution of the chemical diffusion coefficient of lithium in $Li_xN_{0.67}N$ confirms the lithium content has a low impact on Li diffusion (**Figure 6**). Indeed, from the beginning up to the end of the reduction, the D_{Li} values remain in the same order of magnitude. More precisely, two set of data can be distinguished: a mean value of 6×10^{-9} cm2 s^{-1} for the first part of reduction $1.67 \leq x < 1.87$, while D_{Li} is slightly lower near 3×10^{-9} cm^2 s^{-1} for $1.87 < x \leq 2.17$. These D_{Li} values are very

close and consistent with the scarce kinetic data available for lithiated metallic nitride such as 5.6×10^{-9} cm^2 s^{-1} reported for Li_7MnN_4 [34].

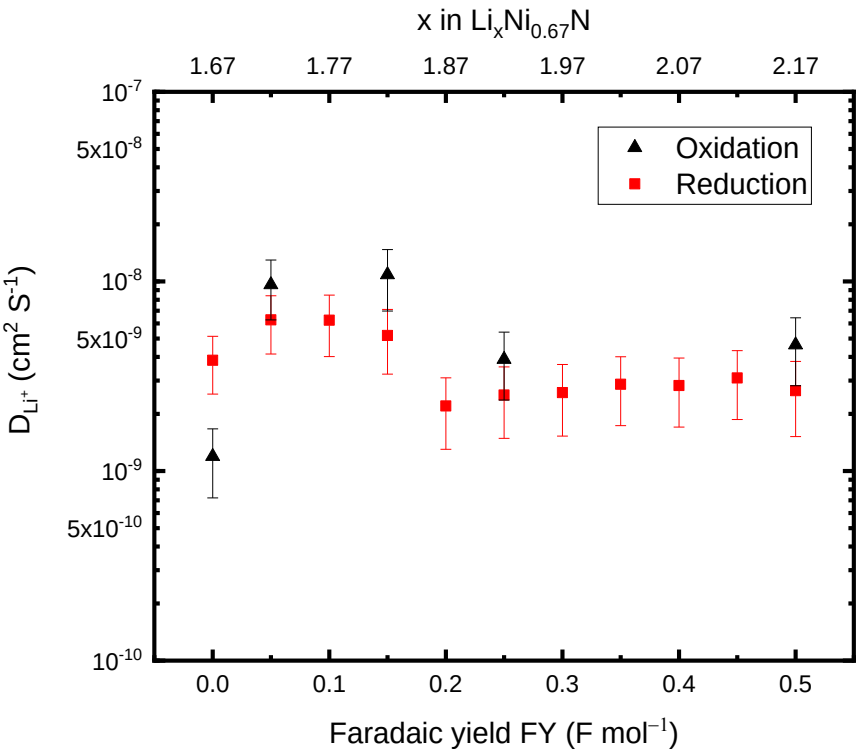

Figure 6. D_{Li} evolution as a function of x in $Li_xNi_{0.67}N$ during reduction and oxidation.

Upon oxidation, the same comment can be made for D_{Li} values, which collectively shift towards higher values but remain very close to the values observed during reduction.

It is interesting to compare the present D_{Li} values and variations in $Li_xNi_{0.67}N$ with the data reported for some well-known high performance layered cathode materials such as $LiNiO_2$ [28, 29], $LiCoO_2$ [30, 31] and $Li(Ni_{1/3}Mn_{1/3}Co_{1/3})O_2$ [37, 38]. The major feature of Li diffusion in $Li_xN_{0.67}N$ is its very moderate x dependence whereas most of Li intercalation

compounds, and especially $LiCoO_2$, $LiNiO_2$, $Li(Ni_{1/3}Mn_{1/3}Co_{1/3})O_2$, exhibit a strong dependence of Li diffusion upon the Li content. Indeed, as reported in [35–40], the lower the Li content in 2D lithiated host material, the higher the apparent chemical diffusion coefficient D_{Li}. For $LiCoO_2$ and $Li(Ni_{1/3}Mn_{1/3}Co_{1/3})O_2$, the variation of D_{Li} is at least of 2 orders of magnitude for a Δx of ≈ 0.5. In the case of $LiNiO_2$ [28, 29], the value of D_{Li} changes by 2 orders of magnitude, obeying to a zig-zag tendency related to its various phase changes. In fact, D_{Li} variations relate closely with the structural changes occurring in the host material upon reduction and oxidation. In the case of LNN, the numerous Li vacancies (0.66 max) available in *2a* sites located in the nitride anions layers can explain the low influence of the Li uptake on the Li diffusion process. As a proof of Li accommodation in *2a* cationic vacancies, a tiny volume cell expansion occurs with a maximum value < 2%. In addition, this volume expansion takes place from x = 1.87, allowing to maintain a high diffusivity by minimizing Li-Li repulsive coulombic interaction. The usually observed slowdown of Li transport with increasing lithium uptake is then strongly limited for LNN (**Figure 6**).

The activation energy for Li diffusion can be then calculated from the slope of the straight-line $Ln\ D_{Li} = f(1/T)$. As shown in **Figure 7**, the Nyquist diagrams of reduced electrodes for x = 1.77 and x = 2.07 are very sensitive to temperature in the 13 °C - 47 °C range (**Figure 7)**. Indeed, when the temperature changes from 13 °C to 47 °C, the electrode impedance is decreasing by a factor of 2 for x = 1.77, from 108 Ω cm² to 51 Ω cm² and by a factor of 4 for x = 2.07, from 136 Ω cm² to only 34 Ω cm². A strong impact is also recorded for the characteristic frequency of the main semi-circle, which decreases with the temperature by a factor of 40 for x = 1.77 and 70 for x = 2.07. The R_2 resistance associated to the SEI formed on the nitride electrode significantly decreases (approximately by a factor of 20) when the

temperature increases, the lowest value of approximately 2 Ω cm² being reached at 47 °C. The corresponding thickness increases with temperature by a factor of 4 for low Li content (x = 1.77) and by a factor of 1.5 for higher Li uptake (x = 2.07) to reach respectively 6.3 nm and 3.5 nm at 47°C. At the same time the frequency range for the Warburg impedance shifts towards higher values when the temperature increases, showing qualitatively an increase in the diffusion rate of lithium ions (**Figure 7**). D_{Li} is calculated for each working temperature and the corresponding Arrhenius plot of Ln (D_{Li}) vs.1/T are displayed for x = 1.77 and x = 2.07 **(Figure S8**).

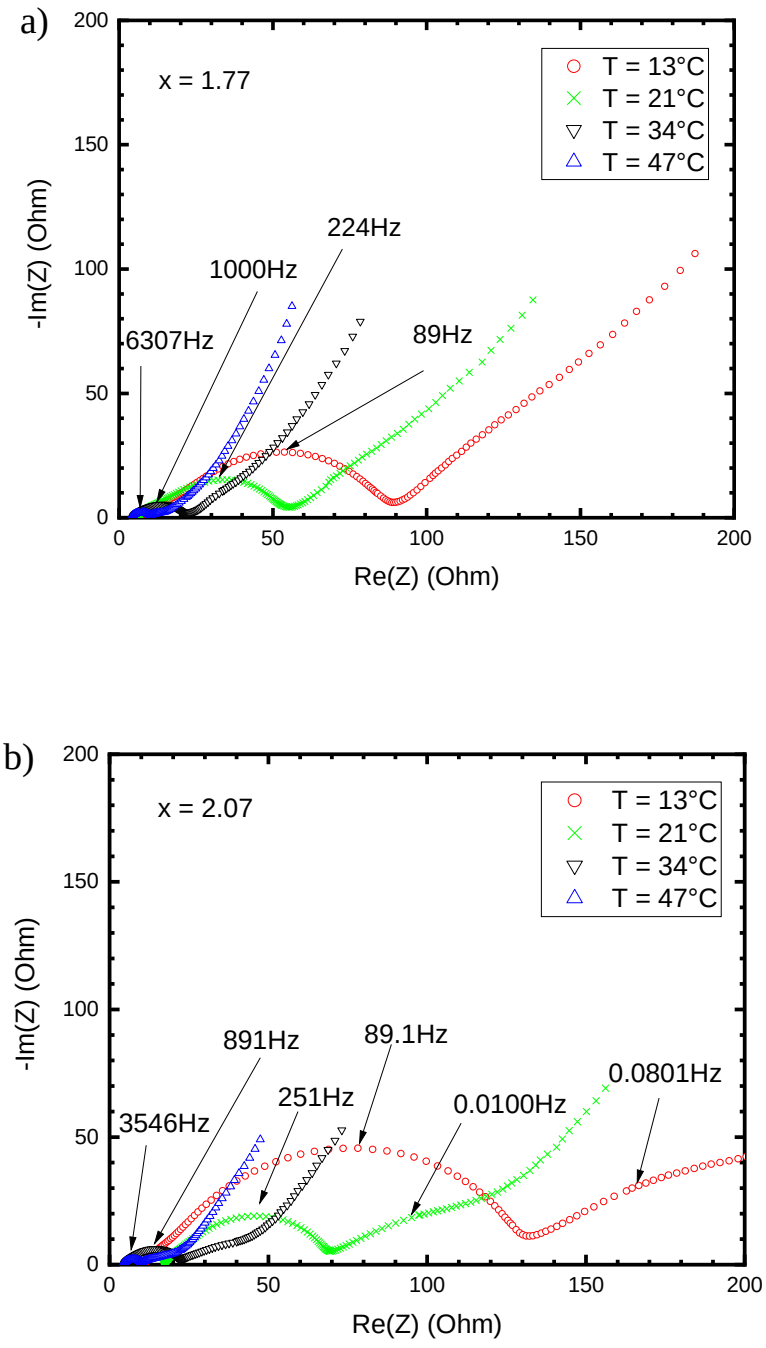

Figure 7. Influence of temperature from 13°C to 47°C on Nyquist diagrams of $Li_xNi_{0.67}N$ electrodes at a) x = 1.77 and b) x = 2.07.

The activation energy for Li diffusion has been calculated from the slope of the straight-line Ln D_{Li} = f (1/T). Values of 0.31 eV and 0.45 eV are found for x = 1.77 and x = 2.07, respectively. This indicates the rate of Li diffusion is not significantly affected by the Li uptake, probably due to the numerous cationic vacancies available for Li accommodation. These values are in good agreement with activation energies reported for Li diffusion in Li intercalation compounds [41]. More precisely, our finding is very close to the activation energy of 0.42 eV reported by Panabiere et al. for Li_7MnN_4[34].

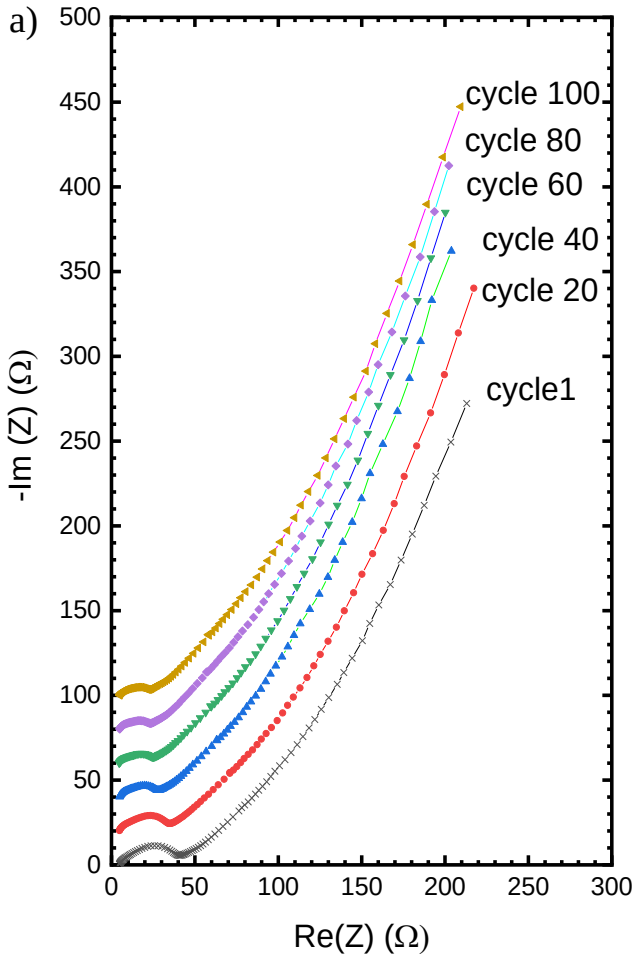

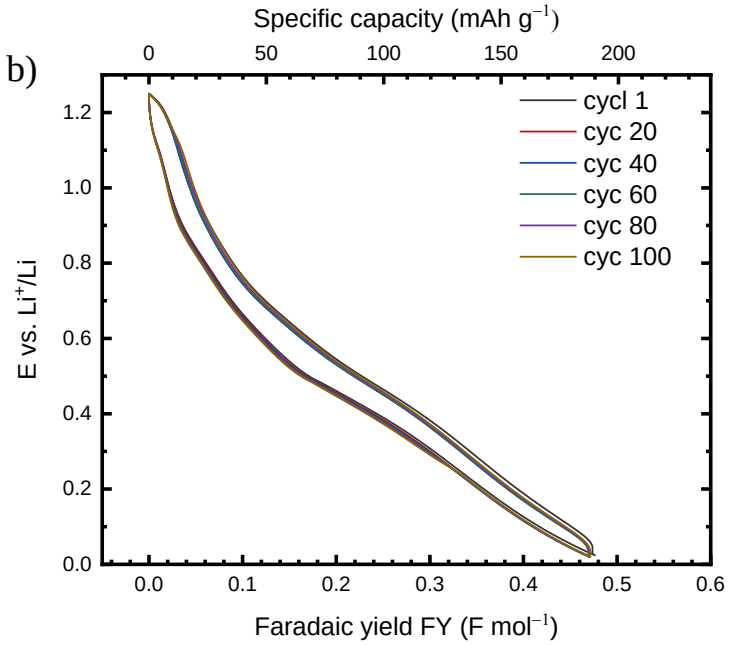

Figure 8. Comparison of impedance diagrams obtained after cycles 1, 20, 40, 60, 80 and 100 at C/10 (40 mA g^{-1}) at room temperature.

The evolution of the impedance spectrum of a LNN-Li cell has been investigated upon cycling at 1C at room temperature. The Nyquist diagrams recorded every 20 cycles from cycle 1 up to cycle 100 are reported in **Figure 8**. All these spectra practically superimpose, showing no significant change occurs in the electrochemical surface area as well as in the charge transfer process, nor in the diffusion process. This result is consistent with the good capacity retention evidenced in **Figure 2b** and the conservation of the galvanostatic profile upon cycles, as shown in **Figure 8b**. The lack of polarization is also explained by a remarkable constant value of |Z| with cycles (**Figure S9a**). A stable resistivity of the SEI formed on nitride is found upon cycles (**Figure S9b)**, indicating the absence of evolution in

the composition or the thickness of this SEI. These results indicate the redox and structural mechanisms do not induce strong structural stress upon repeated reduction-oxidation cycles.

4. Conclusions

A kinetic study of electrochemical Li insertion in LNN has been carried out by impedance spectroscopy as a function of x in $Li_xNi_{0.67}N$, ($1.67 \leq x \leq 2.17$) during the reduction and oxidation process in the 1.25 V-0.02 V voltage range. An equivalent circuit is proposed to simulate the experimental Nyquist diagrams. The fitting results are in good agreement with the experimental data and the parameters of the kinetic process of Li^+ intercalation reaction as well as the respective contributions and characteristics of passivating layers formed on Li and nitride are extracted, using the simulation results. The evolution of the Nyquist diagrams shows a reversible increase in the charge transfer resistance (R_{ct}) from x = 1.77 to the fully reduced electrode (x = 2.17). This resistance is negligible in the oxidized state. Contrary to numerous Li insertion compounds [35–40], the calculated lithium diffusion coefficient, near 5×10^{-9} cm^2 s^{-1}, remains practically stable with the lithium content. Two main structural reasons can explain this kinetic finding: (i) the presence of a large amount of cationic vacancies minimizing repulsive Li-Li interactions and then promoting Li diffusivity (ii) the emergence of a volume change from x = 1.87, also allowing fast Li transport.

Our impedance measurements have also showed the remarkable stability of the SEI layer formed after the first cycle on the LNN electrode, which is advantageous for long cycle life since no electrolyte consumption takes place. The stability of the cell impedance and lithium diffusion coefficient during the reduction-oxidation, as well as the fully reversible evolution of the charge transfer resistance illustrate the “zero-strain” structural behavior of this negative

electrode material allowing to reach a capacity of 200 mAh g^{-1} at C/10, stable over at least 100 cycles.

Acknowledgments

One of the authors (Yanlong Zhou) wishes to thank the CIFRE (no. 2018/1610) funding from Renault.

References

[1] D. Aurbach, Review of selected electrode-solution interactions which determine the performance of Li and Li ion batteries, J. Power Sources. 89 (2000) 206–218. https://doi.org/10.1016/S0378-7753(00)00431-6.

[2] T. Waldmann, B.I. Hogg, M. Wohlfahrt-Mehrens, Li plating as unwanted side reaction in commercial Li-ion cells – A review, J. Power Sources. 384 (2018) 107–124. https://doi.org/10.1016/j.jpowsour.2018.02.063.

[3] T. Ohzuku, A. Ueda, N. Yamamoto, Zero- Strain Insertion Material of Li [Li1 / 3Ti5 / 3] O 4 for Rechargeable Lithium Cells, J. Electrochem. Soc. 142 (1995) 1431–1435. https://doi.org/10.1149/1.2048592.

[4] S. Goriparti, E. Miele, F. De Angelis, E. Di Fabrizio, R. Proietti Zaccaria, C. Capiglia, Review on recent progress of nanostructured anode materials for Li-ion batteries, J. Power Sources. 257 (2014) 421–443. https://doi.org/10.1016/j.jpowsour.2013.11.103.

[5] M. V Reddy, G. V. Subba Rao, B.V.R. Chowdari, Metal Oxides and Oxysalts as Anode Materials for Li Ion Batteries, Chem. Rev. 113 (2013) 5364–5457. https://doi.org/10.1021/cr3001884.

[6] M. Nishijima, N. Tadokoro, Y. Takeda, N. Imanishi, O. Yamamoto, Li deintercalation-intercalation Reaction and Structural Change in Lithium Transition Metal Nitride, Li7MnN4, J. Electrochem. Soc. 141 (1994) 2966–2971. https://doi.org/10.1149/1.2059266.

[7] J. Cabana, C.M. Ionica-Bousquet, C.P. Grey, M.R. Palacín, High rate performance of lithium manganese nitride and oxynitride as negative electrodes in lithium batteries, Electrochem. Commun. 12 (2010) 315–318. https://doi.org/10.1016/j.elecom.2009.12.027.

[8] E. Panabière, N. Emery, S. Bach, J.P. Pereira-Ramos, P. Willmann, Ball-milled Li7MnN4: An attractive negative electrode material for lithium-ion batteries, Electrochim. Acta. 97 (2013) 393–397. https://doi.org/10.1016/j.electacta.2013.03.012.

[9] M. Nishijima, T. Kagohashi, M. Imanishi, Y. Takeda, O. Yamamoto, S. Kondo, Synthesis and electrochemical studies of a new anode material, Li3 - xCoxN, Solid State Ionics. 83 (1996) 107–111. https://doi.org/10.1016/0167-2738(95)00221-9.

[10] M. Nishijima, T. Kagohashi, Y. Takeda, M. Imanishi, O. Yamamoto, Electrochemical studies of a new anode material, Li3-xMxN (M=Co, Ni, Cu), J. Power Sources. 68 (1997) 510–514. https://doi.org/10.1016/S0378-7753(96)02557-8.

[11] T. Shodai, S. Okada, S.I. Tobishima, J.I. Yamaki, Study of Li3-xMxN (M: Co, Ni or Cu) system for use as anode material in lithium rechargeable cells, Solid State Ionics. 86–88 (1996) 785–789. https://doi.org/10.1016/0167-2738(96)00174-9.

[12] T. Shodai, S. Okada, S. Tobishima, J. Yamaki, Anode performance of a new layered nitride Li3-xCoxN (x = 0.2-0.6), J. Power Sources. 68 (1997) 515–518. https://doi.org/10.1016/S0378-7753(97)02597-4.

[13] J.B. Ducros, S. Bach, J.P. Pereira-Ramos, P. Willmann, A novel lithium intercalation compound based on the layered structure of lithium nitridonickelates Li3-2xNixN, Electrochim. Acta. 52 (2007) 7035–7041. https://doi.org/10.1016/j.electacta.2007.05.037.

[14] J.B. Ducros, S. Bach, J.P. Pereira-Ramos, P. Willmann, Layered lithium cobalt nitrides: A new class of lithium intercalation compounds, J. Power Sources. 175 (2008) 517–525. https://doi.org/10.1016/j.jpowsour.2007.09.052.

[15] T. Shodai, Y. Sakurai, T. Suzuki, Reaction mechanisms of Li2.6Co0.4N anode material, Solid State Ionics. 122 (1999) 85–93. https://doi.org/10.1016/S0167-2738(99)00038-7.

[16] J. Yang, Y. Takeda, N. Imanishi, O. Yamamoto, Novel composite anodes based on nano-oxides and Li2.6Co0.4N for lithium ion batteries, Electrochim. Acta. 46 (2001) 2659–2664. https://doi.org/10.1016/S0013-4686(01)00474-1.

[17] J. Yang, Y. Takeda, Q. Li, N. Imanishi, O. Yamamoto, Solid polymer electrolyte cells using SnSb/Li2.6Co0.4N composite anodes, J. Power Sources. 97–98 (2001) 779–781. https://doi.org/10.1016/S0378-7753(01)00607-3.

[18] Y. Liu, K. Horikawa, M. Fujiyoshi, T. Matsumura, N. Imanishi, Y. Takeda, Novel composite anodes based on layered lithium transition metal nitrides for lithium secondary batteries, Solid State Ionics. 172 (2004) 69–72. https://doi.org/10.1016/j.ssi.2004.03.013.

[19] H. Sun, X. He, J. Li, J. Ren, C.Y. Jiang, C. Wan, Hard carbon/Li2.6Co0.4N composite anode materials for Li-ion batteries, Solid State Ionics. 177 (2006) 1331–1334. https://doi.org/10.1016/j.ssi.2006.06.029.

[20] J.B. Ducros, S. Bach, J.P. Pereira-Ramos, P. Willmann, Comparison of the electrochemical properties of metallic layered nitrides containing cobalt, nickel and copper in the 1 V-0.02 V potential range, Electrochem. Commun. 9 (2007) 2496–2500. https://doi.org/10.1016/j.elecom.2007.07.022.

[21] T. Cavoué, N. Emery, N. Umirov, S. Bach, P. Berger, Z. Bakenov, C. Cénac-Morthe, J.P. Pereira-Ramos, Li2.0Ni0.67N, a Promising Negative Electrode Material for Li-Ion Batteries with a Soft Structural Response, Inorg. Chem. 56 (2017) 13815–13821. https://doi.org/10.1021/acs.inorgchem.7b01903.

[22] E. Panabière, N. Emery, S. Bach, J.P. Pereira-Ramos, P. Willmann, Chemical stability of layered lithium cobalt nitrides in air, Corros. Sci. 58 (2012) 237–241. https://doi.org/10.1016/j.corsci.2012.01.032.

[23] E. Panabière, N. Emery, S. Bach, J.P. Pereira-Ramos, P. Willmann, Investigation of the chemical stability of Li7MnN4 in air, Corros. Sci. 77 (2013) 64–68. https://doi.org/10.1016/j.corsci.2013.07.027.

[24] A.C. Larson, R.B. Von Dreele, General structure analysis system (GSAS), Los Alamos Natl. Lab. Tech. Rep. No. LAUR86-748. (2000) 231.

[25] B.H. Toby, EXPGUI , a graphical user interface for GSAS, J. Appl. Crystallogr. 34 (2001) 210–213. https://doi.org/10.1107/S0021889801002242.

[26] L. Guobao, X. Rongjian, L. Chen, The influence of polytetrafluorethylene reduction on the capacity loss of the carbon anode for lithium ion batteries, Solid State Ionics. 90 (1996) 221–225. https://doi.org/10.1016/s0167-2738(96)00367-0.

[27] L. Kavan, Electrochemical Carbon, Chem. Rev. 97 (1997) 3061–3082. https://doi.org/10.1021/cr960003n.

[28] A. Yamada, S. Matsumoto, Y. Nakamura, Direct solid-state synthesis and large-capacity anode operation of Li 3-xFexN, J. Mater. Chem. 21 (2011) 10021–10025. https://doi.org/10.1039/c0jm03735d.

[29] X. Li, J. Xu, P. Huang, W. Yang, Z. Wang, M. Wang, Y. Huang, Y. Zhou, M. Qu, Z. Yu, Y. Lin, In-situ carbon coating to enhance the rate capability of the Li4Ti5O12 anode material and suppress the electrolyte reduction decomposition on the electrode, Electrochim. Acta. 190 (2016) 69–75. https://doi.org/10.1016/j.electacta.2015.12.176.

[30] A. Wei, W. Li, L. Zhang, B. Ren, X. Bai, Z. Liu, Enhanced electrochemical performance of a LTO/N-doped graphene composite as an anode material for Li-ion

batteries, Solid State Ionics. 311 (2017) 98–104. https://doi.org/10.1016/j.ssi.2017.09.017.

[31] A. Purwanto, S.U. Muzayanha, C.S. Yudha, H. Widiyandari, A. Jumari, E.R. Dyartanti, M. Nizam, M.I. Putra, High performance of salt-modified–lto anode in lifepo4 battery, Appl. Sci. 10 (2020) 1–15. https://doi.org/10.3390/app10207135.

[32] A. Zaban, D. Aurbach, Impedance spectroscopy of lithium and nickel electrodes in propylene carbonate solutions of different lithium salts A comparative study, J. Power Sources. 54 (1995) 289–295. https://doi.org/10.1016/0378-7753(94)02086-I.

[33] C. Ho, I.D. Raistrick, R.A. Huggins, Application of A- C Techniques to the Study of Lithium Diffusion in Tungsten Trioxide Thin Films, J. Electrochem. Soc. 127 (1980) 343–350. https://doi.org/10.1149/1.2129668.

[34] E. Panabière, N. Emery, S. Bach, J.P. Pereira-Ramos, P. Willmann, A kinetic study of electrochemical lithium insertion in Li7MnN4 by impedance spectroscopy, J. Alloys Compd. 663 (2016) 624–630. https://doi.org/10.1016/j.jallcom.2015.12.121.

[35] J. Barker, R. Koksbang, M.Y. Saidi, An electrochemical investigation into the lithium insertion properties of LixNiO2 ($0 \leq x \leq 1$), Solid State Ionics. 89 (1996) 25–35. https://doi.org/10.1016/0167-2738(96)00262-7.

[36] Y.M. Choi, S. Il Pyun, S.I. Moon, Y.E. Hyung, A study of the electrochemical lithium intercalation behavior of porous LiNiO2 electrodes prepared by solid-state reaction and sol-gel methods, J. Power Sources. 72 (1998) 83–90. https://doi.org/10.1016/S0378-7753(97)02677-3.

[37] H. Xia, L. Lu, G. Ceder, Li diffusion in LiCoO2 thin films prepared by pulsed laser deposition, J. Power Sources. 159 (2006) 1422–1427. https://doi.org/10.1016/j.jpowsour.2005.12.012.

[38] J. Xie, N. Imanishi, T. Matsumura, A. Hirano, Y. Takeda, O. Yamamoto, Orientation dependence of Li-ion diffusion kinetics in LiCoO2 thin films prepared by RF magnetron sputtering, Solid State Ionics. 179 (2008) 362–370. https://doi.org/10.1016/j.ssi.2008.02.051.

[39] S.-L. Wu, W. Zhang, X. Song, A.K. Shukla, G. Liu, V. Battaglia, V. Srinivasan, High Rate Capability of Li(Ni 1/3 Mn 1/3 Co 1/3)O 2 Electrode for Li-Ion Batteries , J. Electrochem. Soc. 159 (2012) A438–A444. https://doi.org/10.1149/2.062204jes.

[40] V. Charbonneau, A. Lasia, G. Brisard, Impedance studies of Li+ diffusion in nickel manganese cobalt oxide (NMC) during charge/discharge cycles, J. Electroanal. Chem. 875 (2020). https://doi.org/10.1016/j.jelechem.2020.113944.

[41] M. Okubo, Y. Tanaka, H. Zhou, T. Kudo, I. Honma, Determination of activation

energy for Li ion diffusion in electrodes, J. Phys. Chem. B. 113 (2009) 2840–2847. https://doi.org/10.1021/jp8099576.